

Microstructural and textural evolution of pure titanium during differential speed rolling and subsequent annealing

Xinsheng Huang · Kazutaka Suzuki ·
Motohiro Yuasa · Yasumasa Chino

Received: 22 October 2013 / Accepted: 6 January 2014 / Published online: 22 January 2014
© Springer Science+Business Media New York 2014

Abstract The microstructural and textural evolution of pure titanium during differential speed rolling (DSR) at 500 °C and subsequent annealing were investigated using electron backscattered diffraction analysis. Twinning only occurs in the initial stage of DSR, and further deformation is dominated by dislocation slip. The as-rolled microstructure is characterized by large deformed grains, which form a major component of the material, and some dynamically recrystallized (DRXed) grains mainly existing in shear band regions. A dramatic change in the rolling texture, from the transverse direction (TD) split texture with basal poles largely tilted at $\pm 40^\circ$ to the single-peak basal texture, occurs during DSR. This change in texture is accelerated during the late stage of DSR and may be attributed to the gradual lattice rotation of deformed grains caused by enhanced basal slip activity. The basal texture changes back to the TD-split texture with basal poles tilted at $\pm 25^\circ$ after annealing due to consumption of deformed grains with basal orientations from DRXed grains with the TD-split texture. Subsequent extensive grain growth changes the orientation of the *a*-axis from parallel to the TD to parallel to the rolling direction, which is the result of the preferential grain growth in that direction.

Introduction

Commercial pure titanium (cp-Ti) exhibits superb corrosion resistance, is light weight, and can be used in

aerospace, marine, chemical, and biological industries. The preferred orientations of grains strongly affect the mechanical properties and sheet formability of cp-Ti sheets with hexagonal close-packed (HCP) crystal structure. Conventionally rolled cp-Ti sheets tend to exhibit double peaks of basal poles largely tilted at $\pm 35^\circ$ in the transverse direction (TD) (denoted as TD-split texture), which results in a large planar anisotropy and consequent deteriorated sheet formability [1]. It is therefore important to control the rolling texture to achieve cp-Ti sheets with superb formability.

Differential speed rolling (DSR) is an asymmetric rolling process with different rotation speeds for upper and lower rolls. This process results in opposite stress directions for the frictional forces on the upper and lower sheet surfaces and thus induces intense shear strain uniformly throughout the sheet [2]. DSR has a similar effect on shear deformation as equal channel angular extrusion (ECAP), but the potential for satisfying industrial needs is larger for the former [3]. The effects of DSR on the microstructure and mechanical properties of cp-Ti sheets have been recently investigated [1, 4–6]. DSR at elevated temperatures may induce a dramatic orientation change from conventional TD-split texture to a basal texture with a basal pole located roughly at the center of the basal plane pole figure [1, 5]. The change is beneficial in enhancing stretch formability due to increased Lankford value and weakened planar anisotropy originating from texture effects [1]. Heating during shear deformation is necessary to achieve this texture change [1, 5]. Unfortunately, this basal texture in the as-rolled condition is unstable and tends to change to the conventional TD-split texture during subsequent annealing [1].

To control the texture effectively, an in-depth understanding of microstructural and textural evolution during

X. Huang (✉) · K. Suzuki · M. Yuasa · Y. Chino
Materials Research Institute for Sustainable Development,
National Institute of Advanced Industrial Science and
Technology (AIST), Nagoya, Aichi 463-8560, Japan
e-mail: huang-xs@aist.go.jp

rolling and subsequent annealing is needed. Some work has been carried out on revealing microstructural and textural evolution in cp-Ti during conventional cold rolling [7–15] and hot rolling [16–18] for cp-Ti. Extensive twinning occurs in the early stage of cold rolling, whereas dislocation slip dominates deformation in the late stage, resulting in a stable end $\{2\bar{1}\bar{1}5\}\langle 01\bar{1}0\rangle$ orientation [8]. It has been observed that a basal fiber component develops as a secondary texture component at intermediate strains and then disappears at higher strains, the mechanism of which has been suggested to be related to twinning activity [9]. In contrast, twinning activity is relatively restricted when rolling is performed at elevated temperatures [17]. Hot or warm rolling at temperatures below 800 °C results in a texture similar to the cold rolling texture, but the inclination angles of the split basal poles in the TD decrease with increasing rolling temperature [1, 16–18].

Annealing behavior has also been investigated for conventionally cold- and warm-rolled cp-Ti sheets [18–21]. It is well known that annealing changes the orientation by causing a 30° rotation around the *c*-axis with a limited change in the basal pole figure [20]. However, an investigation on the microstructural and textural evolution during multi-pass DSR and subsequent annealing has not been reported in the literature to the best of our knowledge.

In this study, the microstructural and textural evolution during DSR at an elevated temperature and subsequent annealing at different stages was investigated using electron backscattered diffraction (EBSD) analysis. The aim was to elucidate the mechanism for texture formation.

Experimental procedures

DSR was carried out on a commercial-grade hot-rolled cp-Ti sheet (grade 2) with an initial thickness of 3 mm. Shear strain was introduced unidirectionally. The rotation speed of the upper roll was 13.6 m/min and that of the lower roll was 10 m/min, and thus the rotation speed ratio was 1.36. The cp-Ti sheet was heated to 500 °C prior to each rolling pass and neither roll was heated. The rolling direction (RD) for DSR was parallel to the previous RD of the starting material. The cp-Ti sheet was rolled down to 1 mm in thickness by passing it through the rolls 12 times. The reduction per pass was 9 %. The sheet was quenched in water immediately after each pass. A part of the sheet was cut for evaluation after a single pass, 2 passes, 4 passes, 8 passes, and 12 passes. This corresponded to 9, 17, 31, 52, and 67 % in cumulative reduction and also 0.09, 0.18, 0.37, 0.73, and 1.10 in true strain. The samples in the as-rolled condition together with those subsequently annealed at 550 °C for 5 min,

550 °C for 1 h, and 650 °C for 4 h were investigated using EBSD analysis to reveal annealing behavior.

EBSD analyses were carried out on the longitudinal sections of the samples. The measured grain orientations were rotated to be the same as when they are as observed from the rolling plane with an upward RD, which is the common observation direction for pole figures of rolled sheets. The boundaries of $\{10\bar{1}2\}\langle 10\bar{1}1\rangle$ 85° tensile twins, $\{11\bar{2}2\}\langle 11\bar{2}3\rangle$ 65° compression twins, and $\{10\bar{1}1\}\langle 10\bar{1}2\rangle$ 57° compression twins were indicated in the inverse pole figure maps by blue, green, and yellow lines, respectively. In addition, boundaries with misorientation angles larger than 15° were defined as high-angle grain boundaries (HAGB), which are indicated by black lines and were used for the calculation of grain size. Low-angle grain boundaries (LAGB) exhibiting misorientation angles of 4°–15° are indicated by red lines. The twin fractions were calculated by dividing the lengths of the twin boundaries by the length of HAGB. Recrystallized grains and deformed grains were separated using the criterion of grain average misorientation. Grain average misorientation smaller than 0.5°–0.6° indicated recrystallized grains, whereas that larger than 2° indicated deformed grains. The grain sizes, fraction of twins, and Schmid factors were obtained by averaging the results of the EBSD analyses at 3–6 randomly selected square areas with side lengths of 350 μm for each specimen.

Results and discussion

Figure 1 shows the inverse pole figure maps of the starting material and the sheets DSRed at 500 °C after a single pass, 2 passes, 4 passes, 8 passes, and 12 passes. The starting material exhibited an equiaxed microstructure with a grain size of 44 μm. As DSR progresses, equiaxed grains gradually change to elongated grains along the RD due to plastic deformation. Some deformation twins are formed during the initial rolling stage with rolling pass numbers less than 4. During the late rolling stage, specifically after 8 passes, these twins become hardly pronounced.

The formation of twins can be attributed to the large initial grains, though twinning activity generally weakens rapidly with increasing deformation temperature [17]. Tensile twinning mainly occurs within grains (i.e. green and blue grains) with *c*-axes largely tilted from the normal direction (ND) of the sheet, whereas compression twinning mainly occurs within grains (i.e. red grains) with *c*-axes aligned close to the ND. This is a result of the compressive stress components perpendicular and parallel to the *c*-axis, which are favored by tensile twinning and compressive twinning, respectively.

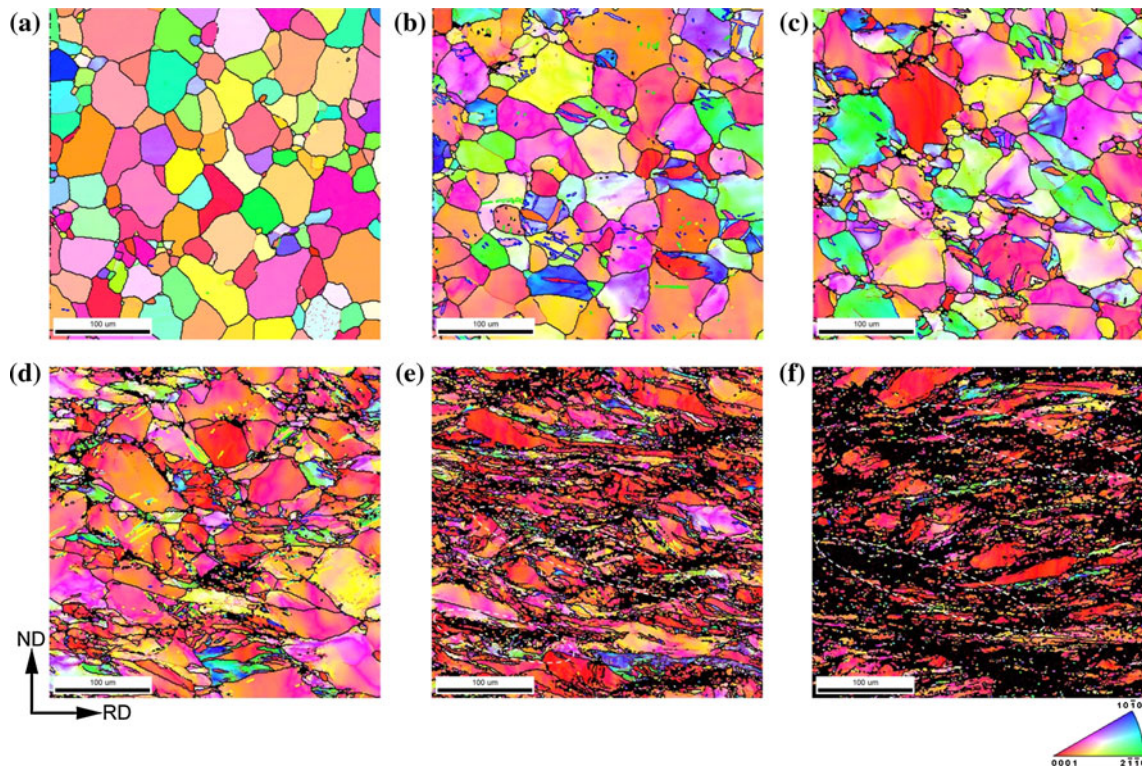
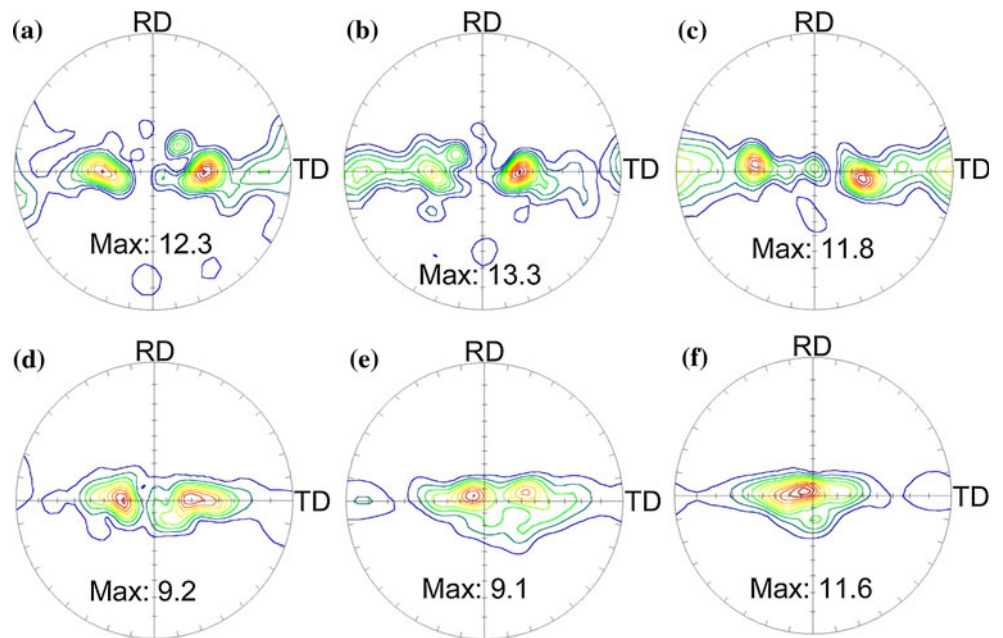


Fig. 1 Inverse pole figure maps of **a** the starting material and the sheets DSRred by **b** a single pass, **c** 2 passes, **d** 4 passes, **e** 8 passes, and **f** 12 passes. The dotted ellipses indicate the shear bands

Fig. 2 (0001) pole figures (intensity level: 1, 2, 3, 4, etc.) of **a** the starting material and the sheets DSRred by **b** a single pass, **c** 2 passes, **d** 4 passes, **e** 8 passes, and **f** 12 passes



In addition, it is obvious that the inverse pole figure map is gradually dominated by the red color as DSR progresses, indicating the development of a basal orientation. Most large elongated grains exhibit a basal orientation, indicating that the development of basal orientation is a result of the gradual lattice

rotation of deformed grains due to slip activity rather than twinning. Shear bands caused by deformation concentration appear in the late rolling stage and develop as DSR progresses.

The (0001) pole figures of the starting material and sheets DSRred by different passes are shown in Fig. 2. DSR

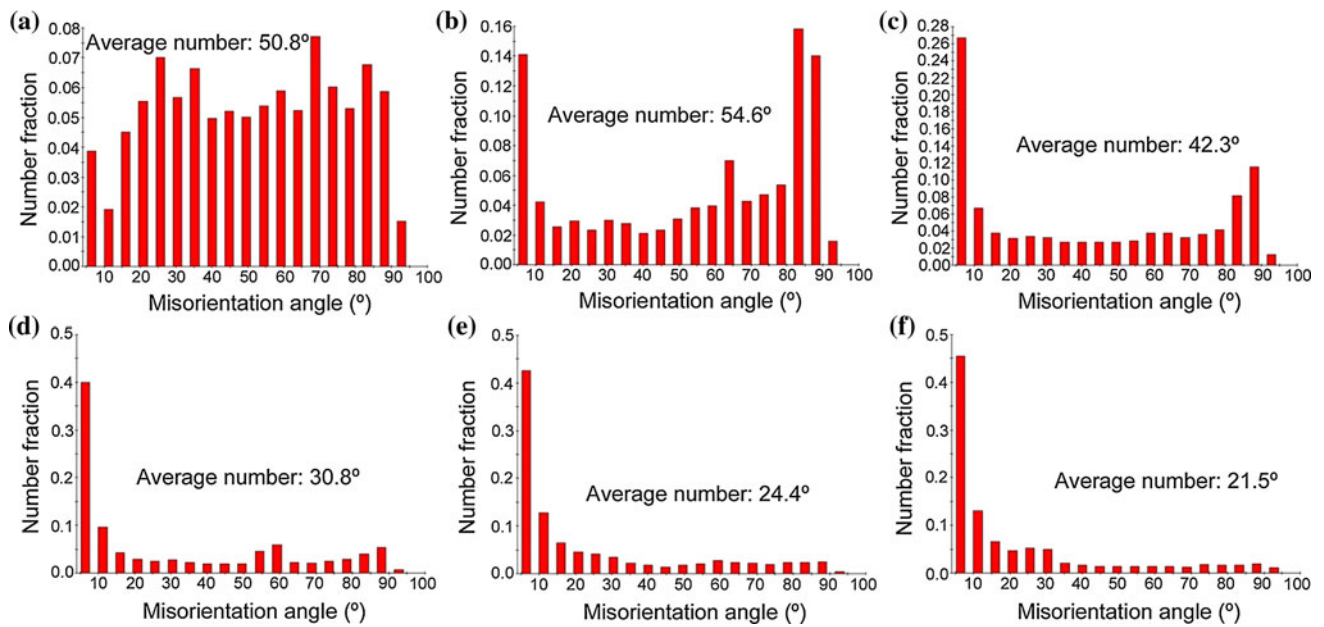


Fig. 3 Distributions of grain boundary misorientation of **a** the starting material and the sheets DSRed by **b** a single pass, **c** 2 passes, **d** 4 passes, **e** 8 passes, and **f** 12 passes

results in a dramatic change from a TD-split double peak texture with the (0001) maxima largely tilted at $\pm 40^\circ$ in the TD to a single-peak basal texture slightly tilted at $\sim 5^\circ$ toward the RD with a large orientation spread in the TD. The inclination angles for the basal poles from the ND toward the TD are about $\pm 40^\circ$, $\pm 35^\circ$, $\pm 40^\circ$, $\pm 28^\circ$, $\pm 20^\circ$, and 0° for the starting material and sheets DSRed by a single pass, 2 passes, 4 passes, 8 passes, and 12 passes, respectively. It appears that the decrease in the inclination angle of the split basal pole and the change to the basal texture occur when subjected to 4 passes and accelerate in the late stage of DSR, specifically after 8 passes.

The distributions of grain boundary misorientation for the starting material and the DSRed sheets are shown in Fig. 3. The starting material exhibits a roughly homogeneous distribution of grain boundary misorientation without distinct peaks. As DSR progresses, the fraction of LAGB increases significantly. In addition, several specific peaks appear for the sheets DSRed by a single pass, 2 passes, and 4 passes. The preferred misorientation angles are 65° and 85° for the sheet DSRed by a single pass, 85° for the sheet DSRed by 2 passes, and 57° and 85° for the sheet DSRed by 4 passes. However, these peaks disappear with further DSR processing.

The changes in grain size and the fractions of deformation twins are summarized in Fig. 4. The grain size decreases from 44 to 11 μm as DSR progresses, and the decrease in grain size starts after 4 passes (see Fig. 4a). The detected $\{11\bar{2}1\}\langle 11\bar{2}6 \rangle$ 35° tensile twins are negligible with quite low fractions (less than 0.2 % for all samples)

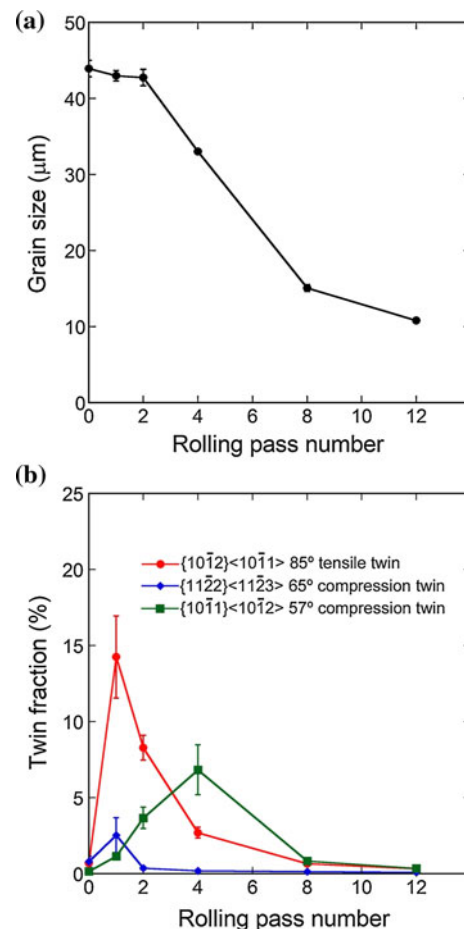
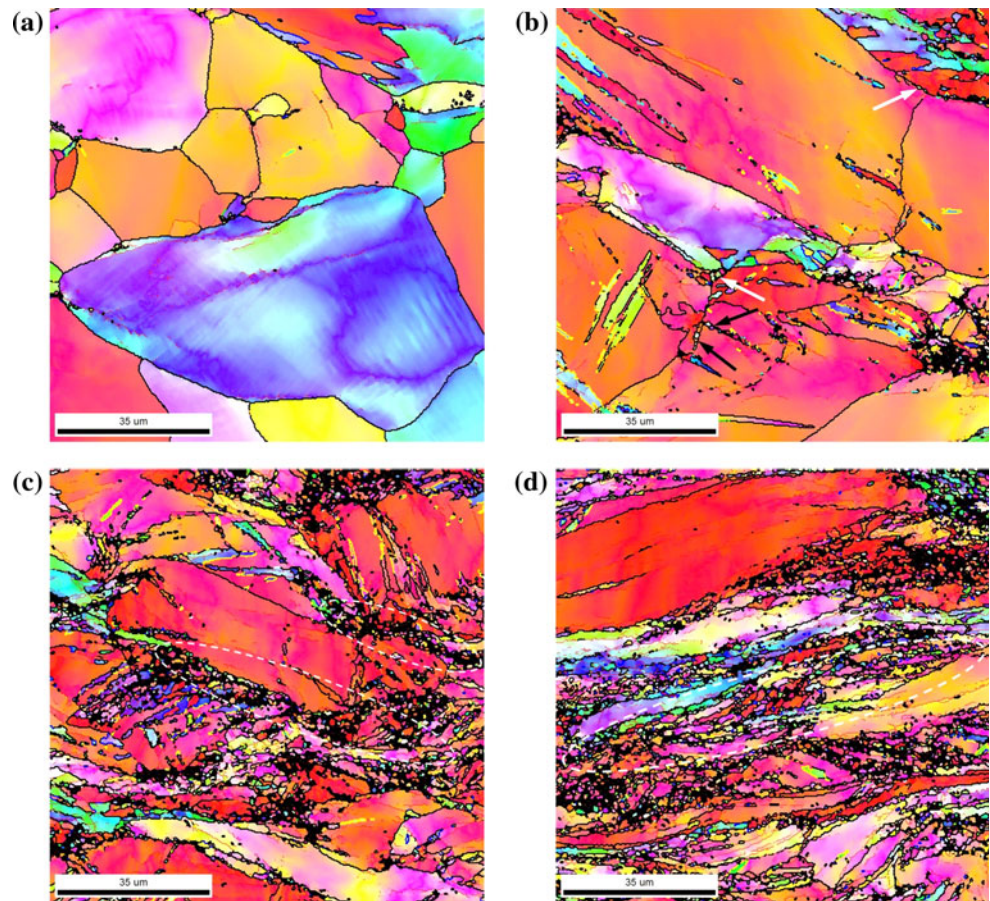


Fig. 4 Changes in **a** grain size and **b** twin fraction as a function of rolling pass number

Fig. 5 Inverse pole figure maps of the sheets DSRed by **a** 2 passes, **b** 4 passes, **c** 8 passes, and **d** 12 passes. The *white* and the *black arrows* indicate DRXed grains at pre-existing grain boundaries and within twins, respectively. The dotted ellipses indicate DRXed grains at the regions of shear bands



and therefore are not shown in Fig. 4b. Figure 4b shows that twinning occurs in the initial rolling stage and becomes ignorable in the late rolling stage. A single-pass DSR generates 85° tensile twins, 65° compression twins, and 57° compression twins with the fractions of 14, 3, and 1 %, respectively. The much higher fraction of 85° tensile twins is due to their lower critical resolved shear stress (CRSS) for twinning and the favored initial orientation compared with the compressive twinning. Further DSR processing rapidly decreases the fraction of 85° tensile twins to 3 % after 4 rolling passes; these twins become undetectable after 12 passes. 65° compressive twinning exhibits a similar tendency for the change in twin fraction, which drops to an undetectable level after 2 passes.

It is interesting to note that 57° compressive twinning exhibits a different behavior. The fraction of 57° compression twins increases as DSR progresses, exhibiting a peak value after 4 rolling passes, before decreasing like the other types of twinning. The fraction of 57° compression twins at the rolling pass number of 4 is 7 %, which is even higher than that (3 %) of 85° tensile twins. The development of a basal orientation component might be one reason for the enhanced 57° compressive twinning. The higher

activity of the 57° compressive twinning compared to that of the 65° compressive twinning supports the previous observation that deformation at elevated temperatures higher than 400°C is favored by the former twinning type [10, 22]. The ignorable twin fraction after 8 passes indicates that deformation is strongly dominated by dislocation slip in the late stage of DSR.

Figure 5 shows the inverse pole figure maps measured at a higher magnification for the sheets DSRed by 2, 4, 8, and 12 passes. This makes it easier to observe dynamic recrystallization (DRX) behavior. DRX is not observed for the sheet DSRed by 2 passes. After 4 passes, DRX appears to start to occur at pre-existing grain boundaries and also within narrow twins. Therefore, DRX, rather than subdivision by deformation twins, causes grain refinement and an inhomogeneous microstructure with a bimodal distribution of grain size. DRXed grains are very fine, having a grain size of $0.8\ \mu\text{m}$. The fraction of DRXed grains obviously increases as DSR progresses. DRX appears to preferentially occur in shear band areas where plastic deformation is localized. The occurrence of DRX after 4 passes is consistent with the rapid decrease in grain size during DSR from 4 passes on, as shown in Fig. 4a. In

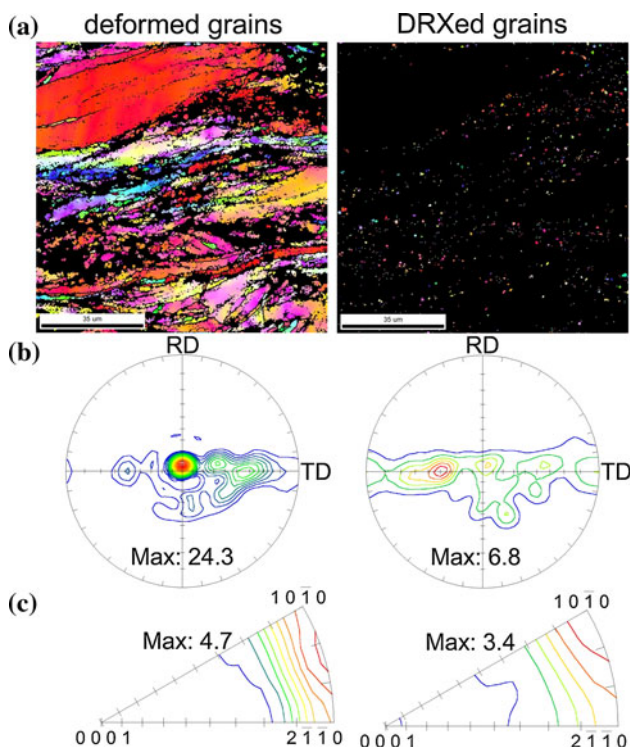


Fig. 6 **a** Inverse pole figure maps, **b** (0001) pole figures (intensity level: 1, 2, 3, 4, etc.), and **c** inverse pole figures observed from the RD (intensity level: 0.5, 1, 1.5, 2, etc.) of deformed grains (left part) and DRXed grains (right part) for the sheet DSRed by 12 passes

addition, very few twins exist in large deformed grains with basal orientations, indicating that deformation is dominated by dislocation slip for those grains.

For the sheet DSRed by 12 passes, the inverse pole figure maps, (0001) pole figures, and inverse pole figures (observed from the RD) associated with both deformed and DRXed grains are shown separately in Fig. 6. It appears that DRXed grains are aligned as bands due to preferential nucleation at the shear bands (Fig. 6a). Deformed grains exhibit a single basal pole with a strong basal texture intensity of 24.3. In contrast, DRXed grains exhibit a different texture. The major texture component of DRXed grains is a pole tilted at $\sim 40^\circ$ in the TD and the texture intensity is remarkably weakened to 6.8 (Fig. 6b). The pole figure looks asymmetrical in the TD with a stronger pole on the left for DRXed grains. This might be due to a statistical problem resulting from the relatively small analyzed area. As shown in Fig. 6c, for both deformed grains and DRXed grains, the $\langle 10\bar{1}0 \rangle$ direction tends to be oriented parallel to the RD, which is a stable orientation for both the cold- and hot-rolled cp-Ti sheets in the as-rolled condition [8–10, 12, 14, 16, 18].

In the present work, deformation twinning only occurs in the initial stage of DSR. Its influence on the global texture is quite limited, as can be confirmed from the small difference between the (0001) pole figure of the

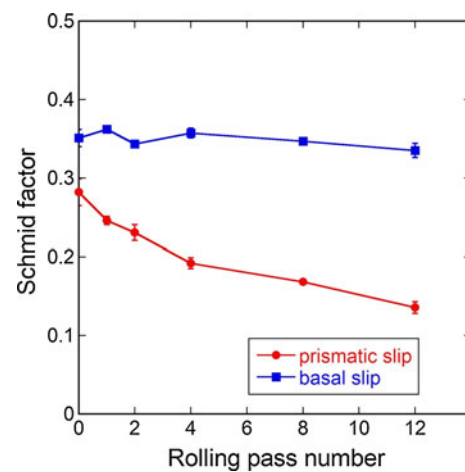


Fig. 7 Changes in Schmid factors for prismatic slip and basal slip as a function of rolling pass number in the case of the loading axis being parallel to the ND

starting material and that of the sheet DSRed by a single pass with the highest fraction of twins (see Figs. 2a, b). In contrast, the texture substantially changes in the late stage of DSR, during which deformation is dominated by dislocation slip. It can therefore be concluded that the change from the TD-split texture to the basal texture is resulted from a lattice rotation of deformed grains induced by dislocation slip.

To roughly evaluate the activities of different slip systems during DSR, the Schmid factors for prismatic slip and basal slip were analyzed under compression along the ND of the sheet for the starting material and the sheets DSRed by 1, 2, 4, 8, and 12 passes, as shown in Fig. 7. The Schmid factor for the pyramidal $\langle c + a \rangle$ slip system was not analyzed because of its much larger CRSS compared with prismatic and basal slip systems for α -Ti [23, 24]. The basal slip system exhibits larger Schmid factors than the prismatic slip system. The favored orientation for basal slip may be attributed to the orientation spread in the TD, especially the component with the c -axes tilted at $\pm 45^\circ$ away from the ND toward the TD, which results in an inclination in the orientation of basal planes with respect to the ND. In contrast, the Schmid factor for prismatic slip exhibits a maximum value for the orientation with the c -axis parallel to the TD and gradually decreases to zero as the c -axis changes its orientation to be parallel to the ND.

Even though the Schmid factors decrease with the progress of DSR for both slip systems due to the shifting of the basal pole toward the ND, it is worth noting that the drop in the Schmid factor is slower for the basal slip system. After 12 passes of DSR, the Schmid factor decreases from 0.36 to 0.34 at a rate of 6 % for the basal slip system, whereas the Schmid factor decreases from 0.28 to 0.14 at a rate of 48 % for the prismatic slip system. Therefore, the ratio

between the Schmid factors of basal and prismatic slip systems correspondingly increases from 1.3 to 2.4 after 12 passes of DSR, suggesting that crystalline orientation becomes more favorable for basal slip as DSR progresses.

Prismatic slip exhibits a lower CRSS and thus a higher activity at low temperatures compared to basal slip in cp-Ti. However, the decrease in the CRSS with increasing deformation temperature is more rapid for basal slip [24, 25]. The ratios between the CRSS of basal slip and prismatic slip at room temperature and at 500 °C are estimated to be 3.6 and 1.5 for Ti, respectively, based on the results reported by Numakura and Koiwa [25]. Comparing a larger value for the ratio of the Schmid factor compared to the ratio of the CRSS between basal slip and prismatic slip for the sheet DSRed by 12 passes at 500 °C (2.4 vs. 1.5), it is assumed that basal slip acts as a major deformation mechanism during the late stage of DSR. In addition, stacking fault energies (SFEs) for basal and prismatic planes are 300 and 150 mJ/m², respectively, for Ti [26]. The higher SFE of the basal plane may induce cross-slip more easily, and, in turn, enhance dynamic recovery. Conversely, the lower SFE of prismatic slip promotes the increase in dislocation density during deformation and thus strain hardening. This would increase the difficulty in the slip on the prismatic planes as further deformation occurs. It is therefore suggested that the formation of a single-peak basal texture is attributed to the enhanced basal slip and in turn the lattice rotation of deformed grains toward basal orientation. This result supports that reported by Suwas et al. [27], in which, using viscoplastic self-consistent simulations to reproduce the experimental shear textures, they found that basal slip is the predominant deformation mechanism during ECAP at 400 °C for cp-Ti.

Even though heating during deformation may enhance non-basal slip activities, the basal texture cannot be achieved by conventional symmetric rolling at the same rolling conditions. In addition, the RD-split double peak component tilted in the RD at $\pm 10^\circ$ to 15° appears besides the conventional TD-split basal poles [1]. The splitting of the basal pole in the RD may be related to the activation of pyramidal $\langle c + a \rangle$ slip, as Agnew et al. [28] suggested for magnesium alloys with the same HCP crystalline structure. Grains with the c -axis tilted at $\pm 45^\circ$ from the ND toward the RD exhibit the maximum Schmid factor for basal slip whereas grains with c -axis orientation nearly parallel to the ND exhibit the maximum Schmid factor for pyramidal $\langle c + a \rangle$ slip under plane strain compression [11]. DSR can generate an additional intense shear force, which results in an inclined resultant force with respect to the ND from the RD. For basal-oriented grains with the c -axes parallel to the ND, the inclined resultant force with respect to the c -axes may increase the Schmid factors for basal slip during DSR. In contrast, the basal orientations are more

favored by pyramidal $\langle c + a \rangle$ slip than basal slip under compressive force during conventional symmetric rolling.

For the sheet DSRed by 12 passes, annealing behavior was investigated using the samples annealed at 550 °C for 300 s, 550 °C for 1 h, and 650 °C for 4 h, corresponding to the initial, intermediate, and full annealing stages, respectively. As shown in Fig. 8, small recrystallized grains and large deformed grains coexist in the sample annealed at 550 °C for 300 s, resulting in a bimodal distribution of grain size and a still high fraction of LAGB. After a longer annealing time (1 h), the fraction of recrystallized grains increases with a notable decrease in the fraction of LAGB. Annealing at 650 °C for 4 h results in a fully annealed microstructure consisting of equiaxed grains without any noticeable abnormal grain growth. The fraction of LAGB further decreases to a very low level, and the peak of the distribution of grain boundary misorientation becomes distinct at 30° as the annealing process progresses (Fig. 8b). The preferential peak at 30° has been frequently observed for rolled metals with a HCP crystal structure, such as cp-Ti [15], magnesium [29], and zirconium alloy [30]. This may be attributed to $\Sigma 13a$ coincidence site lattice (CSL) boundaries with potentially low energies corresponding to a 27.8° rotation around the c -axis [15, 29, 30].

As shown in Fig. 8c, the basal pole located at the center of the (0001) pole figure disappears. Meanwhile, the split basal pole in the TD develops with an inclination angle of $\pm 25^\circ$, and there is a decrease in the orientation spread in the TD after full annealing (Fig. 8c). Even though the basal texture is replaced by the TD-split texture after annealing, the annealed texture exhibits a smaller basal pole inclination angle ($\pm 25^\circ$ vs. $\pm 40^\circ$) compared to the starting material (i.e. commercial hot-rolled sheet) fabricated by conventional hot rolling (see Fig. 2a), which is favored for enhancing sheet formability due to a smaller in-plane anisotropy [1]. In addition, the basal texture intensity remarkably weakens from 11.6 for the as-rolled sheet (see Fig. 2f) to 5.8 at the intermediate stage of annealing and strengthens again to 8.5 after full annealing. It is worth noting that the orientation of the a -axis (i.e. $\langle 2\bar{1}10 \rangle$) changes from parallel to the TD (i.e. $\langle 10\bar{1}0 \rangle // \text{RD}$) to parallel to the RD (i.e. $\langle 2\bar{1}10 \rangle // \text{RD}$) after full annealing (Fig. 8d), which is a 30° rotation around the c -axis as has been frequently observed for conventional cold-rolled cp-Ti sheets during annealing [20].

The image quality (IQ) map measured at a low magnification and the inverse pole figure map measured at a high magnification for the sample annealed at 550 °C for 300 s are shown in Fig. 9. The IQ map allows for easier observation of the distribution of recrystallized grains, which are brighter than deformed grains due to decreased dislocation

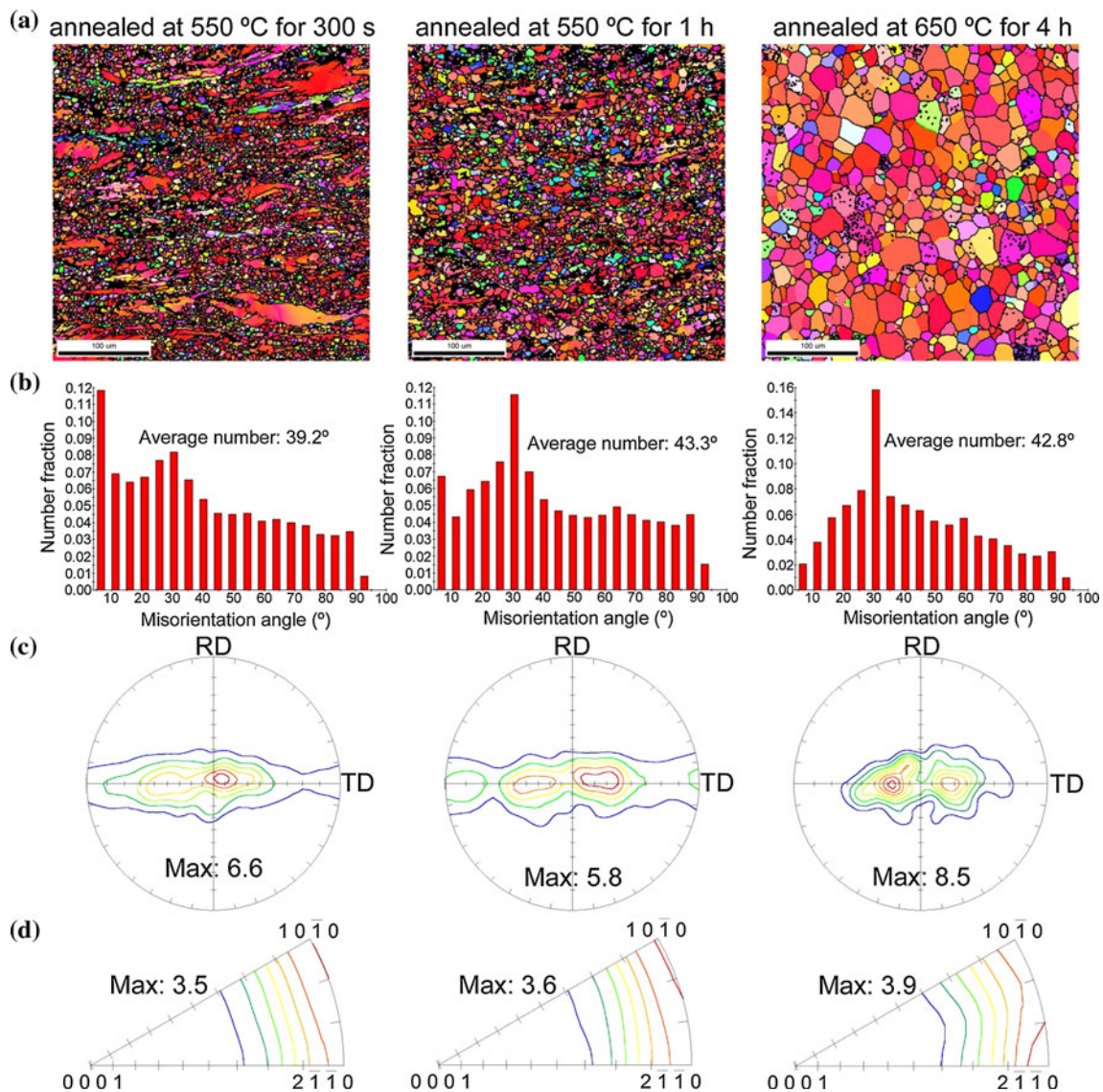


Fig. 8 **a** Inverse pole figure maps, **b** distributions of grain boundary misorientation, **c** (0001) pole figures (intensity level: 1, 2, 3, 4, etc.), and **d** inverse pole figures observed from the RD (intensity level: 0.5,

1, 1.5, 2, etc.) of the samples annealed at 550 °C for 300 s (*left part*), annealed at 550 °C for 1 h (*central part*), and annealed at 650 °C for 4 h (*right part*) for the sheet DSRed by 12 passes

density. It appears that recrystallized grains are aligned along shear bands much like the DRXed grains were in the as-rolled sheet prior to annealing. The inverse pole figure map shows that recrystallized grains around pre-existing grain boundaries with an average grain size of 4.4 μm are consuming large deformed grains with basal orientations. The recrystallized grains exist at similar sites to the DRXed grains in the as-rolled sheet, but the grain size is much larger (4.4 vs. 0.8 μm) compared to the latter. As mentioned above, the basal plane exhibits a higher SFE. This may restrict the increase in dislocation density due to dynamic recovery during rolling and in turn delay static recrystallization (SRX) during subsequent annealing. It is therefore suggested that microstructure evolution is dominated by the

growth of DRXed grains during annealing, which consume large deformed grains with basal orientations before the occurrence of SRX.

The extracted recrystallized grains for the sample annealed at 550 °C for 300 s is shown in Fig. 10. Small recrystallized grains with a grain size of 4.4 μm are aligned as bands (Fig. 10a). The very low fraction of LAGB indicates the successful extraction of recrystallized grains (Fig. 10b). It is noted that recrystallized grains exhibit split basal poles tilted at about ±30° in the TD (Fig. 10c), which is similar to the pole figure after full annealing (see Fig. 8c). This indicates that the change from the single-peak basal texture to the TD-split double peak texture is the result of the recrystallized grain orientations, but not the

Fig. 9 **a** Image quality map and **b** inverse pole figure map of the sheet DSRed by 12 passes and subsequently annealed at 550 °C for 300 s

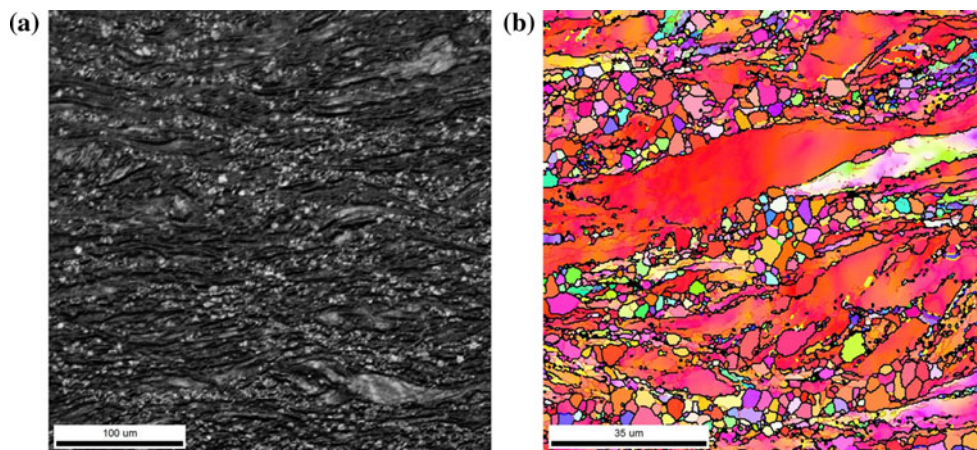
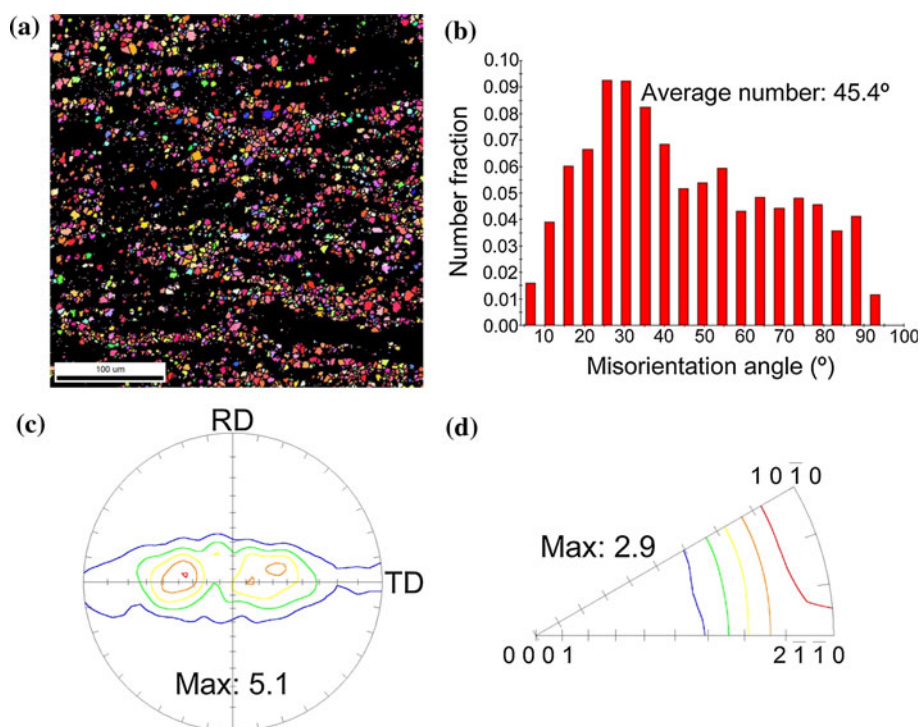


Fig. 10 **a** Inverse pole figure map, **b** distribution of grain boundary misorientation, **c** (0001) pole figure (intensity level: 1, 2, 3, 4, etc.), and **d** inverse pole figure observed from the RD (intensity level: 0.5, 1, 1.5, 2, etc.) of recrystallized grains in the sheet DSRed by 12 passes and subsequently annealed at 550 °C for 300 s



preferential grain growth of specific grains. The texture intensity of recrystallized grains is low (5.1), which results in texture weakening with a decrease in texture intensity from 11.6 to 5.8 during the intermediate stage of annealing. On the other hand, recrystallized grains have a much larger orientation spread in the TD compared to the fully annealed sample. In addition, the inverse pole figure indicates that the recrystallized grains are oriented along $\langle 10\bar{1}0 \rangle // \text{RD}$ (Fig. 10d), which is the same as that of the as-rolled sample, but is different from the fully annealed sample. The shrunk orientation spread in the TD and the change in the orientation of the a -axis may be attributed to subsequent grain growth of recrystallized grains after consuming deformed grains with basal orientations.

To reveal the influence of grain growth on texture evolution, grains with a grain size smaller or larger than the average grain size (19 μm) are separated for the sample fully annealed at 650 °C for 4 h as shown in Fig. 11. Smaller grains and larger grains have grain sizes of 13 and 26 μm , respectively. Both types of grains exhibit similar split basal poles tilted at about $\pm 25^\circ$ in the TD, indicating that grain growth does not change the inclination angle of split basal poles. However, the texture intensity remarkably increases from 6.9 to 10.5 for larger grains compared to smaller grains due to the progress of grain growth. In addition, the orientation spread in the TD is smaller (about $\pm 65^\circ$ vs. $\pm 80^\circ$) for larger grains compared with smaller grains.

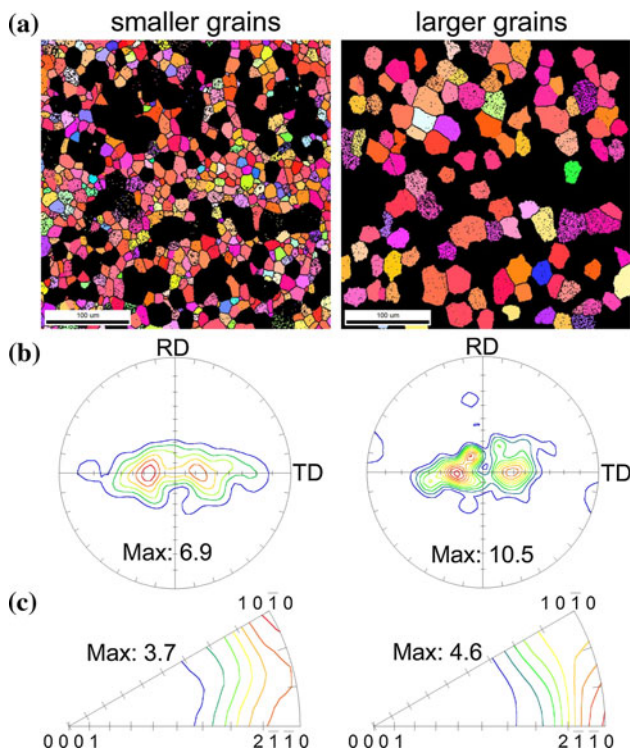


Fig. 11 **a** Inverse pole figure maps, **b** (0001) pole figures (intensity level: 1, 2, 3, 4, etc.), and **c** inverse pole figures observed from the RD (intensity level: 0.5, 1, 1.5, 2, etc.) of grains smaller than (*left part*) or larger than (*right part*) the average grain size (19 μm) for the sheet DSRed by 12 passes and subsequently annealed at 650 $^{\circ}\text{C}$ for 4 h

Considering the above, it is proposed that the texture strengthening is caused by the preferential grain growth of grains belonging to the basal poles tilted at about $\pm 25^{\circ}$ in the TD to consume smaller grains with dispersed orientations close to the TD. For smaller grains, there is a stronger component of the orientation of $\langle 10\bar{1}0 \rangle // \text{RD}$ and a weaker component of the orientation of $\langle 2\bar{1}\bar{1}0 \rangle // \text{RD}$. In contrast, larger grains only exhibit a strong orientation of $\langle 2\bar{1}\bar{1}0 \rangle // \text{RD}$ with a higher intensity (4.6 vs. 3.7). This indicates that the change in the orientation from $\langle 10\bar{1}0 \rangle // \text{RD}$ to $\langle 2\bar{1}\bar{1}0 \rangle // \text{RD}$ originates from the preferential grain growth of the latter texture component.

This phenomenon is similar to texture evolution during grain growth after primary recrystallization for conventionally cold-rolled cp-Ti sheets [20]. Considering the absence of any significant number of CSL boundaries in their results, Bozzolo et al. [20] attributed the orientation change from $\langle 10\bar{1}0 \rangle // \text{RD}$ to $\langle 2\bar{1}\bar{1}0 \rangle // \text{RD}$ RD to a growth advantage for grains belonging to the minor component with an orientation of $\langle 2\bar{1}\bar{1}0 \rangle // \text{RD}$. These grains have fast moving boundaries due to high misorientation angles (larger than 30°) with respect to grains belonging to the major component with an orientation of $\langle 10\bar{1}0 \rangle // \text{RD}$, and

can grow continuously until meeting grains with similar orientations [20]. In this work, the predominant peak at 30° in the distribution of grain boundary misorientation apparently strengthens with grain growth (see Fig. 8b). This phenomenon can be attributed to the increase in $\Sigma 13a$ CSL boundaries. The $\Sigma 13a$ CSL orientation relationship between the minor and major components may enhance the growth rate of the minor component [20]. It is therefore suggested that $\Sigma 13a$ CSL boundaries with low grain boundary energies play an important role on the change in the *a*-axis orientation during grain growth.

In the present work, the orientations of DRXed grains appear to dominate the annealed texture by consuming deformed grains. This results in the change from the single-peak basal texture in the as-rolled condition to the TD-split texture after annealing. It is suggested that the restriction of DRX at shear bands might be effective to persist in the basal texture during annealing, which is favored for enhancing stretch formability.

Conclusions

The microstructural and textural evolution during DSR at an elevated temperature of 500 $^{\circ}\text{C}$ and subsequent annealing for cp-Ti were investigated using EBSD analyses. The main conclusions are as follows:

- (1) Twinning only occurs in the initial stage of DSR and further deformation is dominated by dislocation slip.
- (2) The as-rolled microstructure is largely constituted of large deformed grains and DRXed grains mainly exist in the shear band regions.
- (3) A dramatic texture change from the TD-split texture with basal poles largely tilted at $\pm 40^{\circ}$ to the basal texture occurs during DSR, especially during the late stage. This texture change may be attributed to the gradual lattice rotation of deformed grains caused by enhanced basal slip activity.
- (4) The basal texture changes to a TD-split texture with basal poles tilted at $\pm 25^{\circ}$ after annealing, which is caused by consuming deformed grains with basal orientations from DRXed grains with TD-split texture. Subsequent extensive grain growth results in an orientation change from $\langle 10\bar{1}0 \rangle // \text{RD}$ to $\langle 2\bar{1}\bar{1}0 \rangle // \text{RD}$, which is the result of the preferential grain growth of the latter component enhanced by $\Sigma 13a$ CSL grain boundaries with low boundary energies.

Acknowledgements This work was supported by JSPS KAKENHI Grant Number 24560915.

References

- Huang XS, Suzuki K, Chino Y (2010) Improvement of stretch formability of pure titanium sheet by differential speed rolling. *Scripta Mater* 63:473–476
- Huang XS, Suzuki K, Watazu A, Shigematsu I, Saito N (2008) Microstructure and texture of Mg–Al–Zn alloy processed by differential speed rolling. *J Alloys Compd* 457:408–412
- Huang XS, Suzuki K, Watazu A, Shigematsu I, Saito N (2009) Improvement of formability of Mg–Al–Zn alloy sheet at low temperatures using differential speed rolling. *J Alloys Compd* 470:263–268
- Kim WJ, Yoo SJ, Lee JB (2010) Microstructure and mechanical properties of pure Ti processed by high-ratio differential speed rolling at room temperature. *Scripta Mater* 62:451–454
- Kim WJ, Yoo SJ, Lee JB (2011) Effect of the speed ratio on grain refinement and texture development in pure Ti during differential speed rolling. *Scripta Mater* 64:49–52
- Li ZM, Fu LM, Fu B, Shan AD (2012) Effects of annealing on microstructure and mechanical properties of nano-grained titanium produced by combination of asymmetric and symmetric rolling. *Mater Sci Eng A* 558:309–318
- Lee HP, Esling C, Bunge HJ (1988) Development of the rolling texture in titanium. *Textures Microstruct* 7:317–337
- Inagaki H (1991) Development of cold-rolling textures in pure Ti. *Z Metallkde* 82:779–789
- Bozzolo N, Dewobroto N, Wenk HR, Wagner F (2007) Microstructure and microtexture of highly cold-rolled commercially pure titanium. *J Mater Sci* 42:2405–2416
- Chun YB, Yu SH, Semiati SL, Hwang SK (2005) Effect of deformation twinning on microstructure and texture evolution during cold rolling of CP-titanium. *Mater Sci Eng, A* 398:209–219
- Chun YB, Battaini M, Davies CHJ, Hwang SK (2010) Distribution characteristics of in-grain misorientation axes in cold-rolled commercially pure titanium and their correlation with active slip modes. *Metall Mater Trans A* 41A:3473–3487
- Zherebtsov SV, Dyakonov GS, Salem AA, Malysheva SP, Salishchev GA, Semiati SL (2011) Evolution of grain and subgrain structure during cold rolling of commercial-purity titanium. *Mater Sci Eng A* 528:3474–3479
- Yang DK, An Y, Cizek P, Hodgson P (2011) Development of adiabatic shear band in cold-rolled titanium. *Mater Sci Eng A* 528:3990–3997
- Zhong Y, Yin FX, Nagai K (2008) Role of deformation twin on texture evolution in cold-rolled commercial-purity Ti. *J Mater Res* 23:2954–2966
- Zherebtsov SV, Dyakonov GS, Salem AA, Sokolenko VI, Salishchev GA, Semiati SL (2013) Formation of nanostructures in commercial-purity titanium via cryorolling. *Acta Mater* 61:1167–1178
- Inagaki H (1990) Hot rolling textures in Ti. *Z Metallkde* 81:282–292
- Glavicic MG, Salem AA, Semiati SL (2004) X-ray line-broadening analysis of deformation mechanisms during rolling of commercial-purity titanium. *Acta Mater* 52:647–655
- Chun YB, Hwang SK (2008) Static recrystallization of warm-rolled pure Ti influenced by microstructural inhomogeneity. *Acta Mater* 56:369–379
- Wagner F, Bozzolo N, Van Landuyt O, Grosdidier T (2002) Evolution of recrystallisation texture and microstructure in low alloyed titanium sheets. *Acta Mater* 50:1245–1259
- Bozzolo N, Dewobroto N, Grosdidier T, Wagner F (2005) Texture evolution during grain growth in recrystallized commercially pure titanium. *Mater Sci Eng A* 397:346–355
- Hayama AOF, Sandim HRZ (2006) Annealing behavior of coarse-grained titanium deformed by cold rolling. *Mater Sci Eng A* 418:182–192
- Zeng ZP, Zhang YS, Jonsson S (2009) Microstructure and texture evolution of commercial pure titanium deformed at elevated temperatures. *Mater Sci Eng A* 513–514:83–90
- Chen W, Boehlert CJ, Howe JY, Payzant EA (2011) Elevated-temperature mechanical behavior of as-cast and wrought Ti–6Al–4V–1B. *Metall Mater Trans A* 42A:3046–3061
- Banerjee D, Williams JC (2013) Perspectives on titanium science and technology. *Acta Mater* 61:844–879
- Numakura H, Koiwa M (1998) Dislocations in metals and alloys with the hexagonal close-packed structure. *Metall Sci Technol* 16:4–19
- Gurao NP, Kapoor R, Suwas S (2011) Deformation behaviour of commercially pure titanium at extreme strain rates. *Acta Mater* 59:3431–3446
- Suwas S, Beausir B, Toth LS, Fundenberger JJ, Gottstein G (2011) Texture evolution in commercially pure titanium after warm equal channel angular extrusion. *Acta Mater* 59:1121–1133
- Agnew SR, Yoo MH, Tomé CN (2001) Application of texture simulation to understanding mechanical behavior of Mg and solid solution alloys containing Li or Y. *Acta Mater* 49:4277–4289
- Ostapovets A, Šedá P, Jäger A, Lejček P (2011) Characteristics of coincident site lattice grain boundaries developed during equal channel angular pressing of magnesium single crystals. *Scripta Mater* 64:470–473
- Zhu KY, Bacroix B, Chauveau T, Chaubet D, Castelnaud O (2009) Texture evolution and associated nucleation and growth mechanisms during annealing of a Zr alloy. *Metall Mater Trans A* 40A:2423–2434